Joint Imaging and Communication Using Sparse Antenna Arrays

Nusaibah A. Abusanad*, Mus'ab Ayasrah *, and Hüseyin Arslan*

*Department of Electrical and Electronics Engineering, Istanbul Medipol University, Istanbul, 34810 Turkey
Email:nusaibah.abusanad@std.medipol.edu.tr;musab.alayasra@std.medipol.edu.tr; huseyinarslan@medipol.edu.tr

2024 IEEE Wireless Communications and Networking Conference (WCNC) | 979-8-3503-0358-2/24/$31.00 ©2024 IEEE | DOI: 10.1109/WCNC57260.2024.10571314

***Abstract*—This paper expands sensing capabilities by providing a Joint Imaging and Communication (JIC) system, leveraging millimeter-wave (mm-Wave) technology and sparse antenna array. To address the challenges associated with the high cost and power consumption of dense antenna arrays, we use a sparse antenna array (SAA) to avoid such a problem at the expense of image resolution. The enhancement of acquired image resolution is achieved through the incorporation of multiple low-resolution image components corresponding to distinct transmission-reception combinations. In order to achieve a high level of fairness between communication and imaging performance we formulate a non-convex optimization problem, and then propose an algorithm for finding an approximate solution in a fully digital beamforming case. Numerical results on achievable capacity and image resolution are presented to validate the proposed approach and provide insights into system performance.**

***Index Terms*—Active sensing, digital beamforming, joint imaging and communication, joint sensing and communication, sparse antenna array.**

I. Introduction

THE rollout of commercial 5G networks worldwide has broadened the range of mobile services, extending beyond individual users to include various industries like automotive, smart cities, healthcare, public transportation, and monitoring. These industries rely on three primary 5G use cases: enhanced mobile broadband (eMMB), massive machine-type communication (mMTC), and ultra-reliable and low-latency communication (URLLC). However, these applications are currently limited to communication-related functions. Looking ahead to 6G, there's a recognized need for networks to sense and interact with the physical world, particularly in scenarios like connected vehicles (CV), extended reality (XR), and robotics [1]. Intelligent transportation applications, for example, necessitate intelligent vehicles and traffic monitors that can independently image their surroundings and collaboratively exchange information data, such as microwave traffic images. Thus, enabling communication and radar imaging functionality at the same time reduces hardware resource use significantly. To put it simply, incorporating imaging as an inherent feature becomes a clear necessity in the design of a 6G network architecture.

On one hand, the utilization of wireless signals for imaging is not a novel concept, as it has previously been successfully employed in various contexts such as Wi-Fi [2], millimeter-wave [3], Terahertz wave [4], and radar imaging [5]. On the other hand, recent research has advanced radar imaging and communication system integration, offering waveform designs for dual goals such in [6], [7]. It is worth noting that recent research, as exemplified by [8], has quantified the fundamental performance trade offs inherent in utilizing the same network resources for both imaging and communication. However, a comprehensive integrated communication and imaging system model requires further research in different aspects such as differing requirements concerning waveforms, transceiver advancements, and signal processing algorithms.

The upcoming 6G wireless network is poised to utilize extensive Multiple-Input Multiple-Output (MIMO) Base stations (BS) with numerous antennas, ranging from hundreds to thousands. However, practical constraints like circuit arrangement, power consumption, and computational complexity limit the feasible number of antennas [9]. Incorporating sparse antennas enhances the cost-effectiveness of arrays with a regular geometric structure by significantly reducing the overall number of elements. This reduction is achieved through the use of the theoretical co-array concept, a virtual array model without compromising the array's ability to resolve scatterers or signal sources [10]–[12].

In recent times, sparse arrays have emerged as a valuable tool for advancing radar angular resolution. These arrays are strategically employed to significantly augment the degrees of freedom (DOF) within the context of solving the direction of arrival (DOA) estimation problem while adhering to a predetermined number of physical elements. The consequence of this enhancement is the radar's ability to effectively discern and resolve a greater number of signal sources than the actual count of physical sensors, resulting in a substantial enhancement of the radar's spatial resolution [13], [14]. For an active linear imaging array that uses linear processing at the transmitter and receiver the achievable point spread function (PSF), which characterizes the key properties of a linear imaging system, such as the resolution and side lobe level can be determined by the sum co-array weights. A desired PSF may be synthesized using a technique known as image addition [10], which creates the necessary co-array weighting by combining many images acquired with various transmit-receive beamforming weights.

In this regard, the main contribution of the paper is twofold:

1) We propose a JIC system model based on sparse antenna array (SAA) and then formulate an optimization problem to jointly find the digital transmit and receive beamformers achieving the desired PSF for the imaging system and the channel capacity for communication users.
2) We develop a digital Altmin algorithm for approximately solving the non-convex digital beamformer design problem.

The remainder of the paper is organized as follows. Section II presents the system model. Section III discusses the problem formulation. Simulation results are provided in Section IV, followed by concluding remarks in Section V.

Notation: Matrices are denoted using bold uppercase, vectors using bold lowercase, and scalars using unbolded letters. Superscripts $(.)^{\mathrm{H}}$, $(.)^{\mathrm{T}}$ and $(.)^{\dagger}$ stand for Hermitian transpose, transpose, and pseudo-inverse respectively. The $\mathrm{vec}(.)$ operator stacks the columns of its matrix argument into a column vector. $\mathrm{diag}(.)$, $\mathrm{tr}(.)$ represent the vector formed by the diagonal elements and the trace of the matrix, respectively. The Kronecker and Khatri-Rao products are denoted by $\otimes$ and $\odot$. The Frobenius norm is denoted as $\|.\|_{\mathrm{F}}$.

II. SYSTEM MODEL

Consider a downlink communication and imaging system with a BS, single communication user (CU), and an imaging scene, as shown in Fig.1. The BS is supplied with an N-antenna sparse linear array (SLA), which serves a single antenna CU while imaging the scene at the same time. We focus on active narrow-band sensing of coherent far-field point scatterers. Consider SLA that scans the surrounding environment (a scattering scene) sequentially by broadcasting and receiving focused beams of narrow-band signals in order to generate an image for the scene while also serving CU. Let the number of $\mathrm{N_t}$ indicate the number of transmit antenna while the $\mathrm{N_r}$ is the number of received antenna.

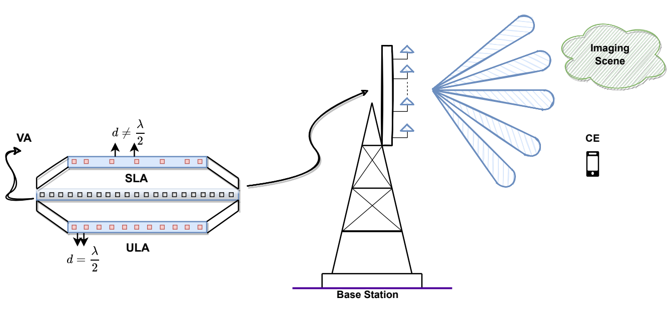

Fig. 1: System Model Joint Imaging and Communication (JIC) and Antenna Configuration.

A. Communication Model

For the communication function, the received signal of the CU can be expressed as

$$\mathbf{y}_c = \mathbf{Hws} + \mathbf{n}, \tag{1}$$

where $\mathbf{n}$ is an AWGN matrix with the variance of each entry being σ^2 and zero mean, $\mathbf{H} \in \mathbb{C}^{(N_t \times N_r)}$ is the downlink channel matrix, which is assumed to be known to the BS, with each entry independently distributed, $\mathbf{w} \in \mathbb{C}^{N_t \times Ns}$ stand for beamforming weight with N_s being the number of data streams, $\mathbf{s} \in \mathbb{C}^{N_s \times 1}$ is the transmitted symbol vector.

With the extended Saleh-Valenzuela model [15], the narrowband mmWave channel matrix can be expressed as

$$\mathbf{H} = \sqrt{\frac{N_t N_r}{L}} \sum_{l=1}^{L} \alpha_l a_r(\theta_{r,l}) a_t^H(\theta_{t,l}), \tag{2}$$

where L represents the number of scattering paths, α_l is the complex gain of the l-th path, and $a_r(\varphi_{r,l}) a_t(\varphi_{t,l})$ denote the receive and the transmit array response vectors, respectively, where $\varphi_{r,l}$ and $\theta_{t,l}$ are the azimuth angle of arrival (AoA) and the angle of departure (AoD) for the l-th. For an ULA, the array response vector can be given as

$$a(\varphi) = [1, e^{j\frac{2\pi}{\lambda}\ d\ \sin(\varphi)}, ..., e^{j\frac{2\pi}{\lambda}\ d\ (N-1)\ \sin(\varphi)}]^T, \tag{3}$$

where d and λ denote the antenna spacing and the signal wavelength, respectively. Without loss of generality, we set $d = \lambda/2$ for ULA and $d \geq \lambda/2$ for SLA. Then the communication performance of the CU can be evaluated by its channel capacity, i.e.,

$$C_u = \log_2(\det(\mathbf{I} + \mathbf{HRH}^H)), \tag{4}$$

where $\mathbf{R}$ is the signal covariance matrix.

B. Imaging Model

We transmit a modulated pulse using the transmit beamforming weight $\mathbf{w_t} \in \mathbb{C}^{N_t}$. The transmitted signals are reflected off the scene and observed by the receiver, then processed by digital beamforming with beamforming weights $\mathbf{w_r} \in \mathbb{C}^{N_r}$. The beamformed signal is then processed using a matched filter yielding

$$y(\mathbf{u}) = \mathbf{w_r}^T(\mathrm{u}) \mathbf{A_r} \Gamma\ \mathbf{A_t}^T \mathbf{w_t}(\mathrm{u}) + \mathbf{n}, \tag{5}$$

where $\mathbf{u} \in \mathbb{R}^3$ is the scan direction, and matrix $\Gamma = \mathrm{diag}(\gamma) \in \mathbb{C}^{K \times K}$ is a diagonal matrix with $\gamma = [\gamma_1, \gamma_2, ..., \gamma_k]^T \in \mathbb{C}^K$ containing the scattering coefficients of the K reflectors. The $N_x \times K$ steering matrix of the T_x or R_x where $x \in \{t, r\}$ is

$$\mathbf{A_x} = [\mathrm{a}_x(\mathrm{v}_1), ..., \mathrm{a}_x(\mathrm{v_K})], \tag{6}$$

where the steering vector $\mathrm{a}_x(\mathrm{v_K}) \in \mathbb{C}^{N_x}$ is evaluated in scatterer direction $\left\{\mathrm{v_K} \in \mathbb{R}^3\right\}_{k=1}^{K}$. Since the scatterer is assumed to be located in the far field, we have $\mathbf{v}_k = [\sin(\varphi)_k \sin(\theta)_k, \cos(\varphi)_k \sin(\theta)_k, \cos(\theta)_k]^T$, where $\varphi_k \in [-\pi/2, \pi/2]$ and $\theta_k \in [0, \pi]$ denote the azimuth and elevation angles of the k_{th}, respectively.

The virtual antenna array (VAA) concept mirrors an actual antenna array, strategically configured to enhance transmission and reception gains, improving overall performance. SAA, with more VAA elements, excels in resolving scatterers compared to a ULA with an equivalent count of physical elements. For instance, a SAA with N components can identify up to

$\mathscr{O}(\mathrm{N}^2)$ sources, while a ULA is limited to $(\mathrm{N}-1)$. Notably, the SAA achieves this with a computational complexity of only $\mathscr{O}(\sqrt{\mathrm{N}})$ for a comparable aperture size [16]. This enhanced source resolution and computational efficiency make SAA appealing for radar, wireless communication, and remote sensing systems with precise localization needs. The sum co-array is a VA model described as a set of pairwise sums of transmit and receive element positions which can be formulated as

$$\mathcal{D}_{\Sigma} = \{\mathbf{d}_t + \mathbf{d}_r | \mathbf{d}_x \in \mathcal{D}_x\}, \tag{7}$$

Here, $\mathcal{D}_x = \{\mathbf{d}_{x,1}, ..., \mathbf{d}_{x,N_x}\} \subset \mathbb{R}^3$. The effective steering matrix $\mathbf{A} \in \mathbb{C}^{N_t N_r \times V}$ is given by

$$\mathbf{A} = \mathbf{A}_t \odot \mathbf{A}_r, \tag{8}$$

where $\mathbf{A}_\mathrm{x} \in \mathbb{C}^{N_\mathrm{x} \times \mathrm{V}}$, for a discrete set of V scatterer directions $\{\mathrm{v}_i\}_{i=1}^{V}$ the effective steering matrix is given by the Kroncker product of the $\mathrm{T_x}$ and $\mathrm{R_x}$ steering vectors evaluated in the direction v_i, i.e., $\mathrm{a}_t(\mathrm{v}_i) \otimes \mathrm{a}_r(\mathrm{v}_i)$. SAA is generally analyzed in the co-array domain. The sum co-array steering matrix $\mathbf{A}_{\Sigma} \in \mathbb{C}^{N_{\Sigma} \times V}$ satisfying

$$\mathbf{A} = \Upsilon^{\mathrm{T}} \mathbf{A}_{\Sigma}, \tag{9}$$

where N_{Σ} is the virtual elements $N_{\Sigma} = |\mathcal{D}_{\Sigma}|$, and Υ is an $N_{\Sigma} \times N_t N_r$ binary matrix such that $\Upsilon : \mathbb{C}^{N_t N_r} \mapsto \mathbb{C}^{N_{\Sigma}}$where

$$\Upsilon_{n,m} = \begin{cases} 1, & \mathbf{d}_{\Sigma,n} = \mathbf{d}_{t,\lceil m/N_r \rceil} + \mathbf{d}_{r,1+(m-1)\bmod N_r} \\ 0, & \text{otherwise} \end{cases} \tag{10}$$

where, $\mathbf{d}_{\mathrm{x},i} \in \mathcal{D}_\mathrm{x}$ denote the elements of the physical array and $\mathbf{d}_{\Sigma,n} \in \mathcal{D}_\mathrm{x}$ the elements of the sum co-array. A visual configuration for SLA, ULA, and the VAA is shown in Fig.1.

To mitigate potential image quality degradation from non-uniform spatial sampling or hardware constraints, multiple component images, each corresponding to distinct transmit-receive antenna weightings, are aggregated. Depending solely on a single transmit-receive weight pair may not always yield high-resolution images. To address this, the concept of image addition involves summing various image components generated using different transmit-receive weight pairs. This technique leverages a beamforming weighting matrix, $\mathbf{W} \in \mathbb{C}^{N_r \times N_t}$, which can be expressed as follows:

$$\mathbf{W} = \sum_{q=1}^{Q} \mathbf{w}_{r,q} \mathbf{w}_{t,q}^T = \mathbf{W}_r \mathbf{W}_t^T. \tag{11}$$

It is pertinent to note that the choice of Q, the number of component images, significantly impacts the duration of the image acquisition process. The Effective PSF is used in a thorough evaluation of the system's capabilities. The Transmit-Receive ($\mathrm{T_x}$-$\mathrm{R_x}$) PSFs, which collectively and in-depth define the imaging system's resolution capabilities and its ability to minimize interference, provide this Effective PSF. In general, PSF is a complex-valued function defined as

$$\psi(\mathbf{u}, \mathbf{v}) = (\mathbf{a}_\mathrm{t}(\mathbf{v}) \otimes \mathbf{a}_\mathrm{r}(\mathbf{v}))^T \mathrm{vec}(\mathbf{W}(\mathbf{u})). \tag{12}$$

The PSF may be expressed as a vector $\psi \in \mathbb{C}^V$ satisfying $\psi = \mathbf{A}^T \mathrm{vec}(\mathbf{W})$. In the same manner, any feasible PSF may be expressed as $\psi = \mathbf{A}_{\Sigma}^T \mathbf{w}_{\Sigma}$, where $\mathbf{w}_{\Sigma} = \Upsilon \mathrm{vec}(\mathbf{W})$.

Finally, the constructed image quality can be evaluated by the peak signal-to-noise ratio (PSNR), i.e.,

$$\mathrm{PSNR} = 10\log_{10}\left(\frac{\max(|\mathrm{J}|^2)}{\frac{1}{N_p}\sum_i |\mathrm{J}_i - \mathrm{R}_i|^2}\right), \tag{13}$$

where J is the radar image, N_p is the total number of pixels in the image, and R_i is the reference signal, on the i-th pixel, obtained with the array [17].

III. PROBLEM FORMULATION

Our goal is to build the digital beamformers in such a way that a high-quality communication link can be created between the BS and CU, while a well-designed PSF can be formulated at the BS to construct an image for the scene. As a result, we consider the following optimization problem

$$\begin{aligned} \min_{\mathbf{W}_x \in \mathbb{C}^{N_x \times Q}, \mathbf{R} \in \mathbb{C}^{(N_t \times N_t)}} \quad & \left\|\psi_{\mathrm{opt}} - A^T \mathrm{vec}(\mathbf{W}_r \mathbf{W}_t^T)\right\|_F^2 + \\ & \left\|\mathbf{R}_{opt} - \mathbf{U}\mathbf{R}\mathbf{U}^T\right\|_F^2 \\ \text{s.t.} \quad & \|\mathbf{W}_x\|_F^2 \leq P_\circ \end{aligned} \tag{14}$$

Where $\mathbf{U}$ is the identity matrix $\in (N_{\Sigma} \times N_t)$ and $\mathrm{P}_\circ$ is the power constraint of the BS. Due to the non-convexity in the objective function. the problem (14) is rather difficult to tackle, while the global minimizer of (14) is in general unattainable, we offer in the following an alternative minimization algorithm approach that can efficiently yield a near-optimal solution to the problem.

A. Proposed Approach

The two variables can be separated, resulting in two sub-problems that are considerably easier to solve.

1) Sub-problem for $\mathbf{W}_r$: By fixing $\mathbf{W}_t$ and solve for $\mathbf{W}_r$, problem (14) is equivalent to

$$\min_{\mathbf{W}_t \in \mathbb{C}^{N_t \times Q},} \quad \left\|\psi_{\mathrm{opt}} - A^T \mathrm{vec}(\mathbf{W}_r \mathbf{W}_t^T)\right\|_F^2 \tag{15}$$

The communication part only depends on $\mathbf{W}_\mathrm{t}$, since it is a downlink communication only. Then this problem can be solved by computing the least square solutions as the following

$$\mathbf{W}_\mathrm{r} = ((\mathbf{A}^T(\mathbf{W}_\mathrm{t} \otimes \mathbf{I}_{N_r}))^{\dagger} \psi_{opt}). \tag{16}$$

2) Sub-problem for $\mathbf{W}_t$: We then fix $\mathbf{W}_\mathrm{r}$ and solve for $\mathbf{W}_\mathrm{t}$ the (14) become

$$\begin{aligned} \min_{\mathbf{W}_t \in \mathbb{C}^{N_t \times Q}, \mathbf{R} \in \mathbb{C}^{(N_t \times N_t)}} \quad & \left\|\psi_{\mathrm{opt}} - A^T \mathrm{vec}(\mathbf{W}_r \mathbf{W}_t^T)\right\|_F^2 + \\ & \left\|\mathbf{R}_{opt} - \mathbf{U}\mathbf{R}\mathbf{U}^T\right\|_F^2 \\ \text{s.t.} \quad & \|\mathbf{W}_t\|_F^2 \leq P_\circ \end{aligned} \tag{17}$$

The problem in (17) is now a summation of two Frobenius norm. Thus, it solves directly using the convex programming (CVX) package.

B. Digital Beamformer Algorithm

Now we are ready to describe the alternative minimization algorithm which has been summarized in Algorithm 1 as follows.

Algorithm 1 Digital Beamformer using Alternative Minimization.

Input: $\mathbf{H}$, ψ_{opt}, $\mathbf{W}_{tinitial}$, $\mathbf{W}_{rinitial}$, $P_{\circ}$, Q, ε_{max}, $k_{\max}$, $\mathbf{R}_{opt}$, $\mathbf{U}$.

Output: W_t, W_r,$\mathbf{R}$

1. $\mathbf{W}_{tinitial}$, $\mathbf{W}_{rinitial}$ are initialized randomly and compute the objective function of 14, denoted as $f^{(0)}$.
2. The tolerable accuracy $\varepsilon_{max} \geq 0$.
3. The maximum iteration number $k_{\max}$, set $k = 1$.

for q=1:Q **do**

while $k \leq k_{max}$ and $\left|f^{(k)} - f^{(k-1)}\right| \geq \varepsilon_{max}$ **do**

4. Compute $\mathbf{W}_{\mathrm{r}}$ by using (16).
5. Compute $\mathbf{W}_{\mathrm{t}}$ by using (17).
6. Compute the objective function f^k based on the obtained variables.
7. $k \leftarrow k + 1$.

return $\mathbf{W}_r$, $\mathbf{W}_t$,$\mathbf{R}$.

In our simulation, the proposed algorithm always converges within tens of iterations.

IV. NUMERICAL RESULTS

In this section, we will delve into a detailed examination of the numerical outcomes obtained through the utilization of the optimization algorithm introduced in the preceding section. Our focus will be directed toward the comprehensive investigation of two distinct linear array models, (ULA) and (SLA). As mentioned previously, our analysis heavily relies on the Maximum Ratio Array (MRA), which boasts the most extensive uniform sum co-array within the specified number of array elements. In our analysis, we consider that all array elements are identical and exhibit omnidirectional characteristics and we do not account for any mutual coupling effects among the array elements. The primary subjects of our study are the ULA configuration with N=11 elements and the MRA setup with N=7 elements. Notably, these two distinct arrays possess equivalent sum co-arrays while spanning the same aperture of 5λ.

To commence our discussion, we shall initially delve into the impact of employing both ULA and SLA configurations on the performance of the imaging system exclusively. The visual representation in the accompanying figure provides a clear insight into the outcomes. When employing the ULA configuration in isolation, with only one image component, we can observe that the desired (PSF) is nearly attained. Conversely, when we incorporate just one image component concurrently with the utilization of the SLA, the resultant image constructed exhibits notably lower resolution as illustrated in Fig. 2.

Fig. (4) provides a visual representation of the performance metrics of JIC system. The key takeaway from this illustration is that achieving the desired PSF necessitates the incorporation

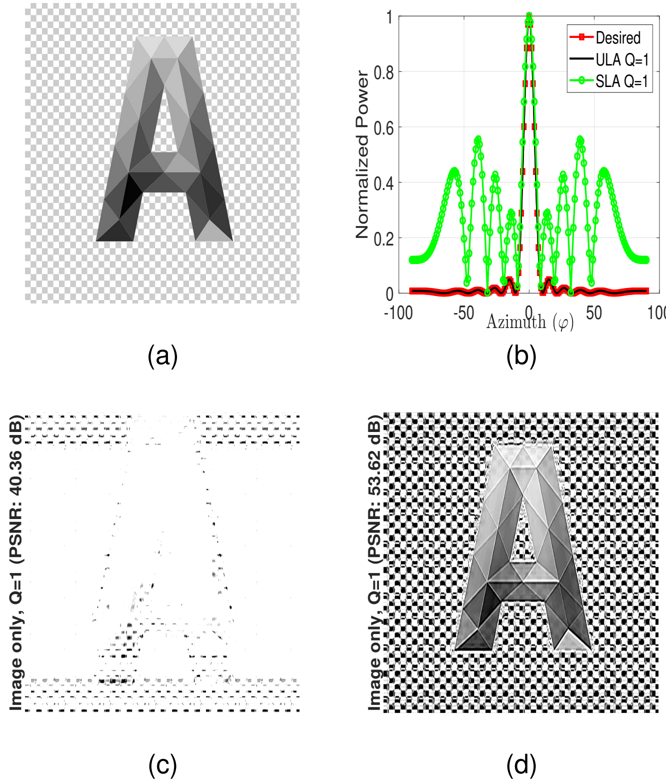

Fig. 2: (a) The scanned image, (b) The normalized PSF for both ULA and SLA when Q=1 (c) The Image of SLA, (d) The Image of ULA.

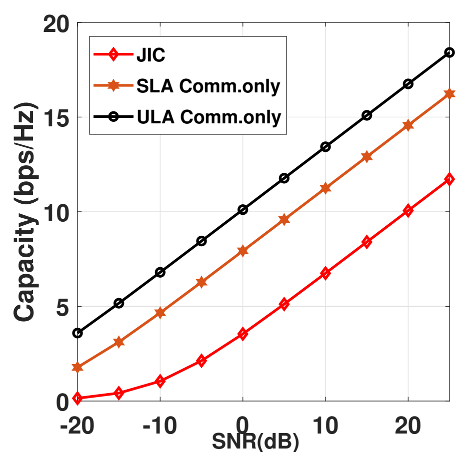

Fig. 3: Capacity (bps/Hz).

of approximately five image components. This observation carries significant implications for the practical utility of such a system model across a range of applications. The JIC system concept is adaptable to a wide range of applications, allowing image components to be customized to meet unique needs. processing complexity is related to Quality of Service (QoS) requirements, with applications emphasizing high-resolution

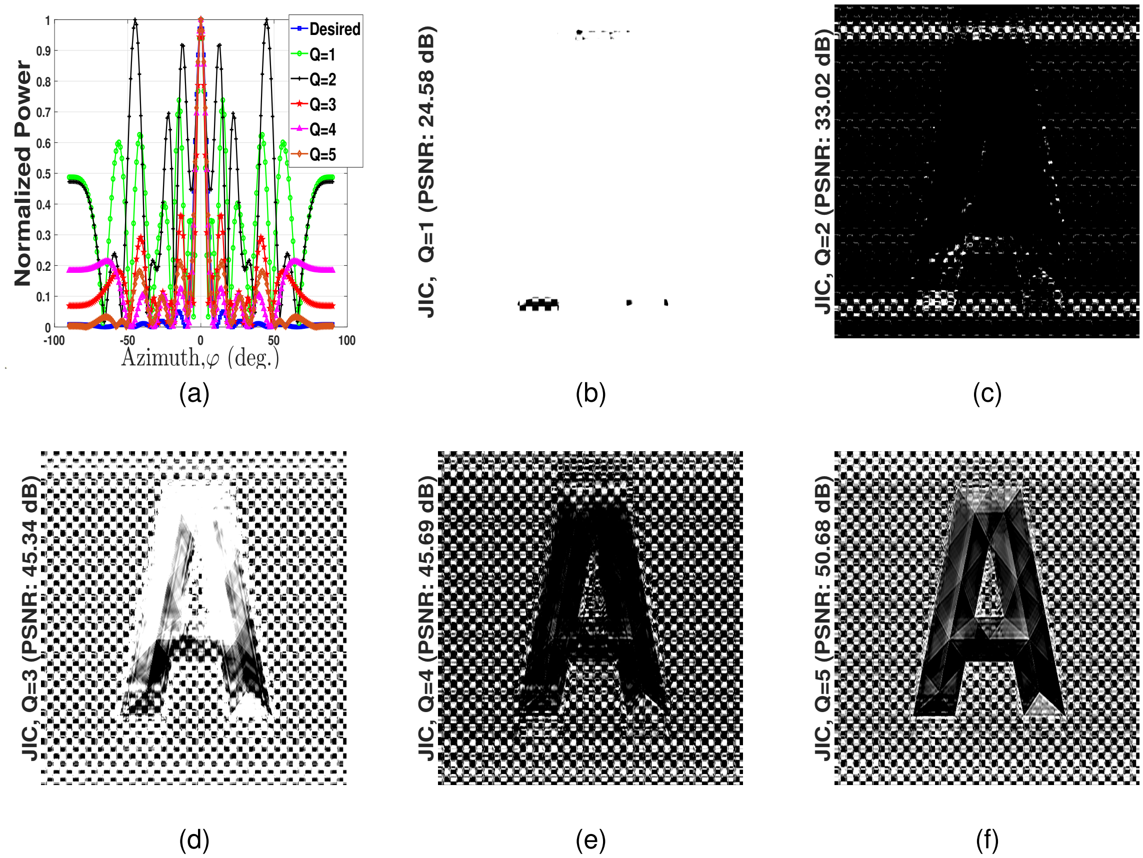

Fig. 4: (a) Normalized PSF for JIC, (b) Q=1, (c) Q=2, (d) Q=3, (e) Q=4, (f) Q=5.

images requiring more processing power. This results in a trade-off between complexity and image resolution, which affects processing power and acquisition time. When compared to ULA, the JIC-based SLA system offers advantages for applications that accept lower-resolution images by reducing power consumption and simplifying setups. However, there is a trade-off that affects communication user capacity, as shown in Fig. (3).

The visual representation of the generated image is directly correlated with Peak signal-to-noise ratio (PSNR) values. Higher-resolution images are associated with higher PSNR values, indicating better image quality. Conversely, lower-resolution images have lower PSNR values, reflecting lower image quality.

V. CONCLUSION

This paper investigated a system model that combines imaging and communication using a sparse antenna array. The goal is to address the complexity and power consumption issues associated with the usage of a uniform linear array. This method also allows for image resolution to be adjusted based on the application's individual requirements. It is crucial to highlight, however, that these benefits come at the expense of lower capacity for communication users.

The proposed system model could be expanded in future studies to include alternative beamforming strategies, such as analog and hybrid beamforming. This extension would entail looking at how various methods affect the number of low-resolution images needed to create a high-resolution image. The model might also be extended to more general (MIMO) scenarios with a larger number of communication users to investigate the impact of inter-user interference on the overall system.

VI. ACKNOWLEDGEMENT

This work was supported by the Scientific and Technological Research Council of Turkey (TUBITAK) under Grant 120C142.

REFERENCES

[1] A. Liu, Z. Huang, M. Li, Y. Wan, W. Li, T. X. Han, C. Liu, R. Du, D. K. P. Tan, J. Lu, Y. Shen, F. Colone, and K. Chetty, "A survey on fundamental limits of integrated sensing and communication," *IEEE Communications Surveys Tutorials*, vol. 24, no. 2, pp. 994–1034, 2022.

[2] Y. He, D. Zhang, and Y. Chen, "High-resolution WiFi imaging with reconfigurable intelligent surfaces," *IEEE Internet of Things Journal*, vol. 10, no. 2, pp. 1775–1786, 2023.

[3] J. Guan, A. Paidimarri, A. Valdes-Garcia, and B. Sadhu, "3-D imaging using millimeter-wave 5g signal reflections," *IEEE Transactions on Microwave Theory and Techniques*, vol. 69, no. 6, pp. 2936–2948, 2021.

[4] A. M. Molaei, S. Hu, V. Skouroliakou, V. Fusco, X. Chen, and O. Yurduseven, "Fast image reconstruction for near-field terahertz imaging with multistatic non-uniform sparse arrays," in *Radar Sensor Technology XXVII*, vol. 12535. SPIE, 2023, pp. 264–272.
[5] H. Ren, Z. Sun, J. Yang, Y. Xiao, H. An, Z. Li, and J. Wu, "Swarm uav sar for 3-D imaging: System analysis and sensing matrix design," *IEEE Transactions on Geoscience and Remote Sensing*, vol. 60, pp. 1–16, 2022.
[6] S. Hwang, J. Seo, J. Park, H. Kim, and B. J. Jeong, "Compressive sensing-based radar imaging and subcarrier allocation for joint MIMO OFDM radar and communication system," *Sensors*, vol. 21, no. 7, p. 2382, 2021.
[7] K. Zhu, J. Wang, X. Liang, L. Chen, Y. Li, X. Bu, and Y. Wu, "Joint SAR imaging and wireless communication using the FBMC chirp waveform," *Science China Information Sciences*, vol. 63, pp. 1–3, 2020.
[8] N. Mehrotra and A. Sabharwal, "On the degrees of freedom region for simultaneous imaging & uplink communication," *IEEE Journal on Selected Areas in Communications*, vol. 40, no. 6, pp. 1768–1779, 2022.
[9] E. Björnson, L. Sanguinetti, H. Wymeersch, J. Hoydis, and T. L. Marzetta, "Massive mimo is a reality—what is next?: Five promising research directions for antenna arrays," *Digital Signal Processing*, vol. 94, pp. 3–20, 2019.
[10] R. T. Hoctor and S. A. Kassam, "The unifying role of the coarray in aperture synthesis for coherent and incoherent imaging," *Proceedings of the IEEE*, vol. 78, no. 4, pp. 735–752, 1990.
[11] M. Wang and A. Nehorai, "Coarrays, MUSIC, and the Cramér–Rao bound," *IEEE Transactions on Signal Processing*, vol. 65, no. 4, pp. 933–946, 2016.
[12] R. Rajamäki, S. P. Chepuri, and V. Koivunen, "Analog beamforming for active imaging using sparse arrays," in *2019 53rd Asilomar Conference on Signals, Systems, and Computers*. IEEE, 2019, pp. 1202–1206.
[13] A. M. Ahmed, U. S. K. P. M. Thanthrige, A. E. Gamal, and A. Sezgin, "Deep learning for DOA estimation in MIMO radar systems via emulation of large antenna arrays," *IEEE Communications Letters*, vol. 25, no. 5, pp. 1559–1563, 2021.
[14] S. Yang, W. Lyu, Z. Zhang, and C. Yuen, "Enhancing near-field sensing and communications with sparse arrays: Potentials, challenges, and emerging trends," *arXiv preprint arXiv:2309.08681*, 2023.
[15] N. González-Prelcic, R. Méndez-Rial, and R. W. Heath, "Radar aided beam alignment in mmwave v2i communications supporting antenna diversity," in *2016 Information Theory and Applications Workshop (ITA)*, 2016, pp. 1–7.
[16] R. Rajamäki and V. Koivunen, "Sparse low-redundancy linear array with uniform sum Co-array," in *ICASSP 2020 - 2020 IEEE International Conference on Acoustics, Speech and Signal Processing (ICASSP)*, 2020, pp. 4592–4596.
[17] A. Beni, L. Miccinesi, and M. Pieraccini, "Comparison between compressive sensing and non-uniform array for a MIMO GBSAR with elevation resolution: Simulations and experimental tests," *Electronics*, vol. 12, no. 5, p. 1100, 2023.